Influence of the Sacrificial Polystyrene Removal Pathway on the TiO$_2$ Nanocapsule Structure

Nelly Hérault, and Katharina M. Fromm*

Department of Chemistry, University of Fribourg, Chemin du Musée 9, CH-Fribourg,
e-mail: katharina.fromm@unifr.ch

This study demonstrates the significant influence of the polystyrene removal pathway on the TiO$_2$ nanocapsules obtained from PS@TiO$_2$ core-shell particles. In a first step, the polystyrene spheres were coated with titanium oxide via hydrolysis and condensation of the titanium precursor to form PS@TiO$_2$ core-shell particles. Then, the creation of the empty cavity to form TiO$_2$ nanocapsules was achieved by removing the polystyrene template by *i*) thermal decomposition of the polystyrene or *ii*) dissolution of the polystyrene using *Soxhlet* extractor followed by a thermal procedure. These pathways to remove the polystyrene were investigated by thermogravimetric studies, IR spectroscopy, transmission and scanning electron microscopy and powder X-ray diffraction. The final TiO$_2$ nanocapsule structure strongly depends on the sacrificial polystyrene removal pathway. The preservation of the TiO$_2$ nanocapsules was obtained essentially when the polystyrene was dissolved before the crystallization of the TiO$_2$.

Keywords: TiO$_2$ Nanocapsules, Synthesis, Polystyrene decomposition, Polystyrene dissolution.

Introduction

Inorganic hollow structures (*e.g.* TiO$_2$,[1 – 3] SiO$_2$,[4] ZnO,[5] Fe$_3$O$_4$,[6] SnO$_2$,[3] CeO$_2$[7]) have attracted much attention since the past decades for their special properties in photocatalysis, sensors, Li-ion batteries, or drug delivery.[1][2] This morphology provides a high surface area, low density, effective light harvesting, and particular optical, electrical, mechanical, photo-electrochemical, and catalytic properties among others.[1][2] Moreover, the void space confers high cargo loading/releasing capacity interesting for drug, peptides or other biological molecule delivery systems.[1][2][8] Three different routes of synthesis are known for obtaining hollow structures materials. The sacrificial hard template method is based on the formation of core-shell particles where the core (*e.g.* carbon,[9] polymer,[3][7][10] silica[11][12]) is removed either by thermal treatment or by etching in an appropriate solvent. This last step is crucial and often the main drawback of this synthetic route. The use of soft templates (such as micelles, vesicles) for making capsules facilitates the elimination of the core.[1] However, this approach leads to a poor control on morphology and monodispersity of the final particles. The last route corresponds to a 'template-free' synthesis involving *in-situ* dissolution/recrystallization processes based on the *Ostwald* Ripening mechanism.[1] This process combines the advantages of both hard and soft template syntheses, but nevertheless this method is less investigated.

Titanium oxide materials are highly used in sun cream, paints, pigments, in the biomedical field,[13] and in photocatalysis.[14][15] In particular, the semiconductor properties of TiO$_2$-based materials revealed a broad research interest in the fields of solar cells,[15 – 17]photo-electrochromics, or photocatalysis,[15][18] *e.g.* water splitting,[19][20] photoreduction of CO$_2$,[20] or water purification.[21] However, these intrinsic properties highly depend on the shape, the size, and the crystallinity of TiO$_2$.

TiO$_2$ nanocapsule synthesis mostly involves sacrificial hard template spheres where the titanium oxide is coated on their surface. This template may be constituted by an organic polymer[10][22] (as polystyrene or co-block polymers) or inorganic compound such as silica[11] which is easily removable. The polystyrene (PS) is one of the most common sacrificial templates because the diameter of the spheres is tunable and the polystyrene is easily removed by thermal decomposition or by dissolution in an organic solvent such as THF,[23] xylene containing triethylamine,[8] or toluene.[3][10] However, *Imhof*[10] has observed a deformation of TiO$_2$ shells after dissolving PS in toluene from PS@TiO$_2$ core-shell particles followed by a drying step, while the capsules remained spherical after

calcination, causing however damages to the TiO$_2$ shells. *Pei et al.*[8] studied the encapsulation of Triclosan in TiO$_2$ nanocapsules formed from PS@TiO$_2$ core-shell particles. For obtaining the capsules the PS was dissolved in triethylamine-containing boiling xylene (bp = 138 – 145 °C) for 12 h. The resultant capsules were compact, with smooth surface and undamaged. For comparison, they treated the core-shell particles by thermal treatment at 500 °C for 3 h resulting in TiO$_2$ particles with damaged shells. They attributed this damage to the crystalline transition of TiO$_2$ and the contraction of the capsules.

THF Was used for the dissolution of the PS from core-shell particles by *Demirörs et al.*[23] showing good efficiency for the elimination of PS for thin TiO$_2$ wall thicknesses. Unfortunately, upon increasing the wall, the dissolution of PS was not efficient anymore and the core remained inside the material.

Numerous articles have been published in this field, involving thermal decomposition of PS or its dissolution into different solvents at room temperature or at the boiling point of it. But the dissolution of PS using solid/liquid extraction system which is a simple and soft method for removing the polymer core was never studied.
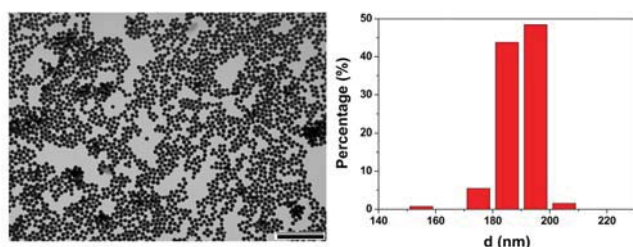
Figure 1. TEM picture and size distribution of polystyrene spheres, scale bar represents 2 μm.

The goal of this study was the evaluation of the removal pathway of the polystyrene from PS@TiO$_2$ on the final titanium oxide nanocapsule structure. The thermal decomposition under air of the polystyrene template with simultaneous crystallization of the TiO$_2$ was compared to its dissolution in chloroform using *Soxhlet* apparatus followed by the crystallization of TiO$_2$ upon calcination.

Results and Discussion

Titanium oxide nanocapsules were formed by coating of titanium oxide on polystyrene spheres that were used as sacrificial templates.

The synthesis of anionic polystyrene spheres was inspired by *Kartsonakis et al.*[24] and corresponds to the emulsion polymerization of styrene monomer. The polystyrene beads have a spherical shape with an average diameter of 190 nm as shown in *Fig. 1*. These PS spheres were coated with TiO$_2$ by hydrolysis/condensation of titanium isopropoxide occurring on the surface of the PS (*Scheme 1*).

In order to obtain hollow TiO$_2$ nanocontainers from the PS@TiO$_2$ core-shell particles, two methods exist in the literature which are *i*) the calcination of the powder above the temperature of the PS decomposition[8][10]or *ii*) the dissolution of PS in a solvent. To get rid of the PS the material is ageing in solvent at room temperature or at the boiling point of the solvent. A simple method was never studied for this purpose: the dissolution of PS by liquid-solid extraction using a *Soxhlet* apparatus.

This method allows the renewability of fresh solvent and the elimination of PS residues during the different cycles' draining of the thimbles without any mechanical forces applied on the material. For this soft method, the ideal solvent should well dissolve
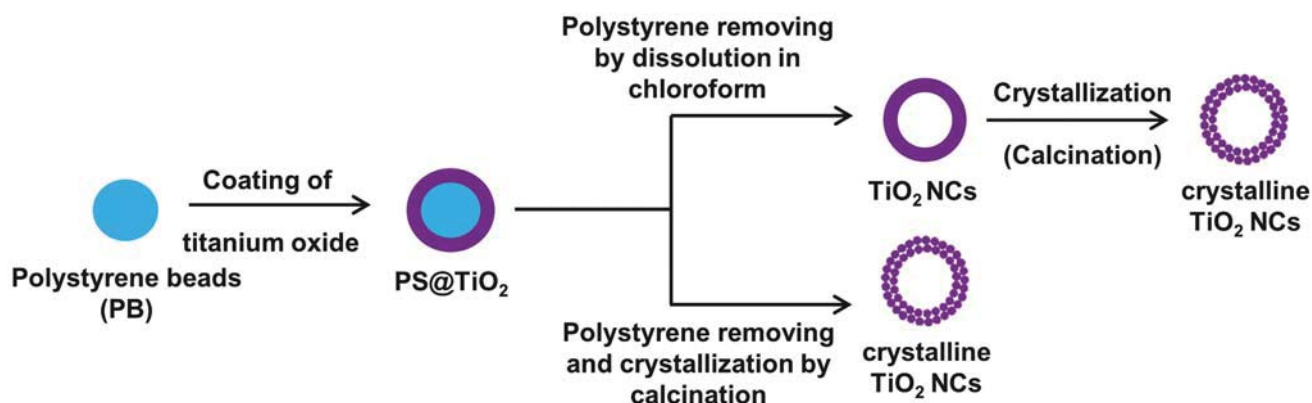
Scheme 1. Synthetic pathways for the TiO$_2$ nanocapsule formation.

the PS (as in the other methods) and possess a low boiling point.

Compared to other solvents, chloroform is a promising candidate for dissolving the polystyrene using a *Soxhlet* extractor due to the combination of both properties summarized in *Table 1*.

In this study, the decomposition of the polystyrene (PS) by thermal treatment (PS@TiO$_2$-1) was compared to the dissolution of PS in chloroform using a solid/liquid extractor followed by thermal treatment (PS@TiO$_2$-2).

According to the TGA analysis of PS@TiO$_2$ (*Fig. 2*), the total decomposition of the PS occurred below 450 °C. Moreover, the decomposition of the PS after

Table 1. Polystyrene solubility and boiling point of potential solvents

Solvent	PS solubility [g/ml][31]	Boiling point [°C]
Toluene	0.68	111
Tetrahydrofuran	0.96	66
Xylene	0.40	138 − 145
N,N-Dimethylformamide	0.31	153
Chloroform	1.28	61
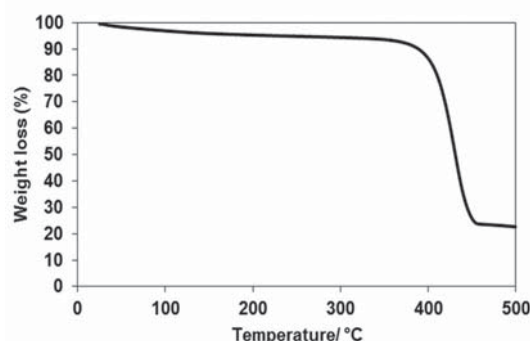
**Figure 2.** TGA of PS@TiO$_2$ before the removal treatment of PS (as synthesized).
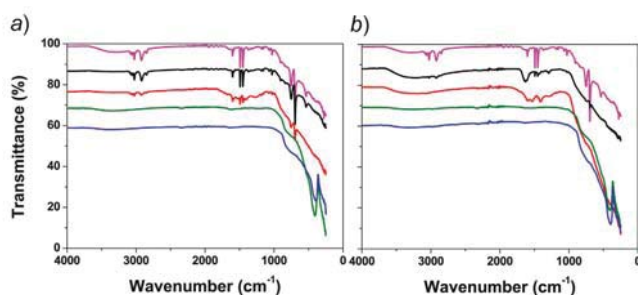
Figure 3. Infrared spectra of PS@TiO$_2$ as synthesized (pink), after calcination at 300 °C (black), 400 °C (red), 500 °C (green), and 700 °C (blue) (A) PS@TiO$_2$-1 and (B) PS@TiO$_2$-2.

the different treatments (calcination or dissolution of PS followed by calcination) was studied by IR spectroscopy (*Fig. 3*). The spectrum which corresponds to PS@TiO$_2$ (pink curve) before treatment shows strong bands between 500 and 1950 cm^{-1} and 2845 − 3085 cm^{-1} which originate from polystyrene[25] and a large band between 2500 and 3500 cm^{-1} and one around 1630 cm^{-1} corresponding to the stretching and bending vibration of hydroxyl groups.[26] For the thermally treated sample for removing the PS, called PS@TiO$_2$-1 (*Fig. 3a*), before and after calcination at 300 or 400 °C, the polystyrene was still present and the band of the hydroxyl group was drastically reduced. From 500 °C onwards, the bands of polystyrene totally vanished. Moreover, new bands were observed in the 400 − 900 cm^{-1} region that can be attributed to the O−Ti−O vibration mode of anatase.[26]

In the case of the dissolution of PS before the calcination treatment, which corresponds to the sample PS@TiO$_2$-2 (*Fig. 3b*), after calcination at 300 °C and 400 °C, the bands attributed to PS were present but in much lower intensity, confirming the partial dissolution of the PS in chloroform. Above 500 °C, the PS was not detectable anymore and the band belonging to the anatase phase appeared,[26] which is in agreement with the X-ray results showing the presence of anatase (see *Fig. 6*, below).

The thermal influence on the TiO$_2$ NC shape was followed by SEM. *Fig. 4* corresponds to the SEM
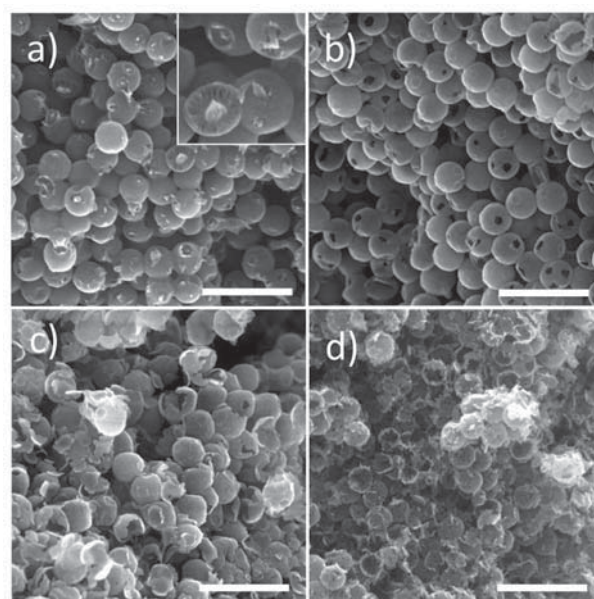
Figure 4. Thermal study of PS@TiO$_2$-1 after calcination at *a*) 300 °C, *b*) 400 °C, *c*) 500 °C, and *d*) 700 °C, scale bar represents 1 μm.

3

pictures of PS@TiO$_2$-1 after different temperatures of calcination at which the PS was thermally decomposed. As shown in *Fig. 4a*, the decomposition already started at 300 °C, leading to a breaking of the shells of the TiO$_2$. From the inlay zoom picture of *Fig. 4a*, the inside of nanocapsules shows that part of the polystyrene is left in lamellar form inside the TiO$_2$ nanocapsules, while at 400 °C (*Fig. 4b*), the TiO$_2$ nanocapsules were in majority drilled by the PS passing through. This phenomenon led to the loss of the nanocapsule structure at 500 °C which was confirmed at 700 °C where only debris of TiO$_2$ nanocapsules is obtained.

Fig. 5 shows the SEM pictures of PS@TiO$_2$-2 after the dissolution of PS in chloroform following different calcination temperatures on the way to obtain TiO$_2$ in its anatase phase. Before the thermal treatment, the TiO$_2$ nanocapsules were undamaged and the cavity was already formed as it is shown by the TEM picture on *Fig. 5b*. Until 500 °C, their structure was preserved
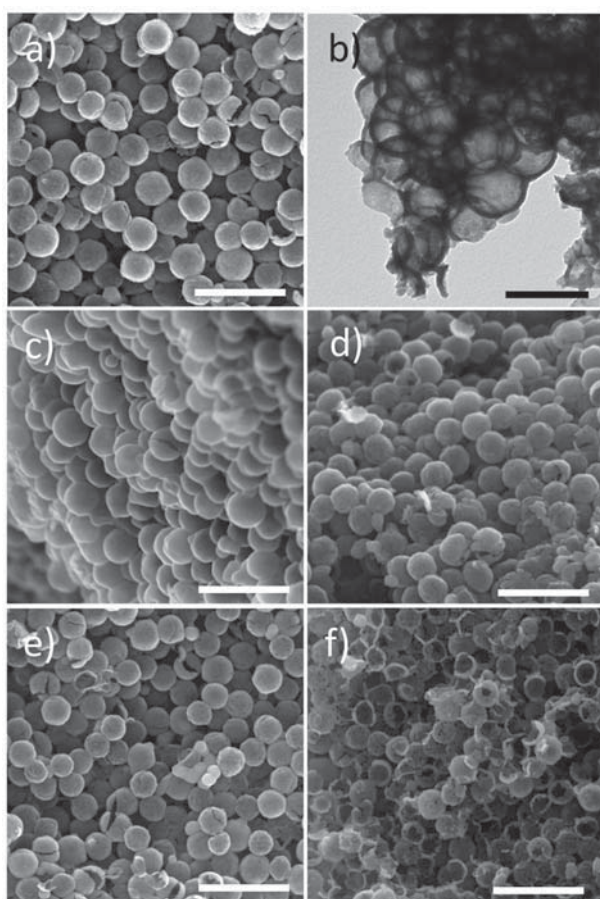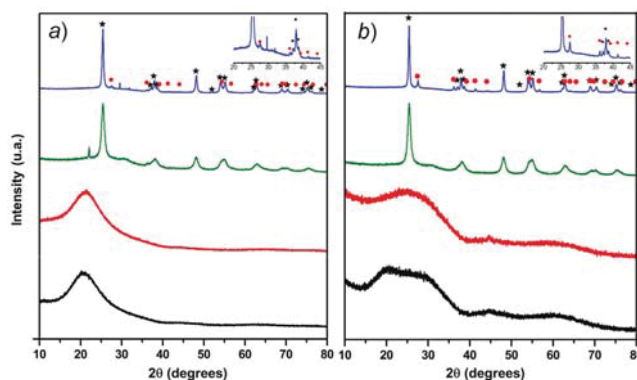
unlike during the previous process. Unfortunately at 700 °C, the final TiO$_2$ was found as debris of nanocapsules like for PS@TiO$_2$-1 when the PS was thermally decomposed. The loss of the structure at 700 °C could be due to the growth of TiO$_2$ crystallites forming the nanocapsule structure. Indeed, the crystallization of the amorphous TiO$_2$ to anatase occurred between 400 and 500 °C according to the X-ray diffraction which showed the presence of the anatase phase after calcination at 500 °C. Between 500 and 700 °C, the TiO$_2$ phase transition from anatase to rutile partially occurred as shown in *Fig. 6*, which is in accordance with the literature where the transition phase starts around 600 °C under air in most of the cases.[27]

After the TiO$_2$ crystallization between 400 and 500 °C, the crystallites were growing with the increase of the calcination temperature. Using the *Scherrer* equation, the determination of crystallite sizes was performed from diffractograms (*Table 2*). At 500 °C, TiO$_2$ corresponds to the anatase phase with crystallite sizes of around 9 nm for PS@TiO$_2$-1 and PS@TiO$_2$-2. While at 700 °C, the anatase crystallites are around 18 and 23 nm and the rutile crystallites around 15 and 22 nm in diameter for PS@TiO$_2$-1 and PS@TiO$_2$-2, respectively. The growth of the crystallites is due to their sintering under thermal conditions.

From *Rietveld* refinement of the diffractograms of PS@TiO$_2$-1 and PS@TiO$_2$-2 after 700 °C (*Figs. S1* and *S2*), the ratio anatase-to-rutile was determined (A/R). It showed a ratio of 98:2 for PS@TiO$_2$-1 while the ratio was 86:14 for PS@TiO$_2$-2 (*Table 2*). The kinetic of anatase-to-rutile transformation depends on several parameters because it is a reconstructive process and these factors have impact on the time-temperature conditions.[27] For instance, the particle size and shape, the surface area, the impurities and the

Figure 5. SEM pictures of PS@TiO$_2$-2 *a*) after PS dissolution and calcination at *c*) 300 °C, *d*) 400 °C, *e*) 500 °C, *f*) 700 °C, and *b*) TEM pictures of PS@TiO$_2$-2 after PS dissolution, white and black scale bars represent 1 μm and 250 nm, respectively.

Figure 6. X-ray diffractograms after 300 °C (black), 400 °C (red), 500 °C (green), and 700 °C (blue) for (A) PS@TiO$_2$-1 and (B) PS@TiO$_2$-2 (black stars: anatase phase; red dots: rutile phase).

Table 2. TiO$_2$ crystallites size calculation of PS@TiO$_2$-1 and PS@TiO$_2$-2 after calcination at 500 and 700 °C

	Calcination at 500 °C		Calcination at 700 °C		
	Anatase	Rutile	Anatase	Rutile	Ratio A:R[a]
PS@TiO$_2$-1	*ca.* 9 nm	–	*ca.* 18 nm	*ca.* 15 nm	98:2
PS@TiO$_2$-2	*ca.* 9 nm	–	*ca.* 23 nm	*ca.* 22 nm	86:14

[a] Determination using *Rietveld* refinement.

conditions of the transformation (atmosphere, heating rate,...) play a role in the transformation kinetic.[27]

We assume that the loss of the TiO$_2$ NC shape at 700 °C for PS@TiO$_2$-2 is coming from the sintering of the crystallites which firstly could create holes in the shell and finally lead to the structural collapse when the diameter of the crystallites reaches the wall thickness of TiO$_2$ (around 20 nm) as it is proposed in *Scheme 2*.

The decomposition of polystyrene by calcination drilled the TiO$_2$ nanocapsules starting from 300 °C while the structure of TiO$_2$ as nanocapsules was preserved until 500 °C by dissolving the polystyrene in chloroform, before the phase transition of TiO$_2$ under thermal treatment.

These differences in shape could influence other properties such as the band gap energy of the material which is one important parameter for a semiconductor.

The absorption edge of TiO$_2$ for the four different samples is shown in *Fig. 7a*. This edge is redshifted for PS@TiO$_2$-1 compared to PS@TiO$_2$-2, indicating a decrease of the bandgap. Moreover, for PS@TiO$_2$-1 after 500 °C, a broad band appears in the visible range. The band gap energies were estimated from the modified *Kubelka-Munk* method[28][29] (*Fig. 7b*) considering indirect transition.

For both materials, no drastic change was observed depending on the temperature of calcination (3.17 *vs.* 3.14 and 3.26 *vs.* 3.27 eV for PS@TiO$_2$-1 and PS@TiO$_2$-2). In the literature, the common value for anatase is around 3.2 eV, while for rutile, it is around 3.0 eV.[15][21] Surprisingly, the PS@TiO$_2$-1 has the lowest E_{GAP} value for both temperatures while it has the highest A/R ratio after 700 °C (*Table 3*). This behavior is not well understood.
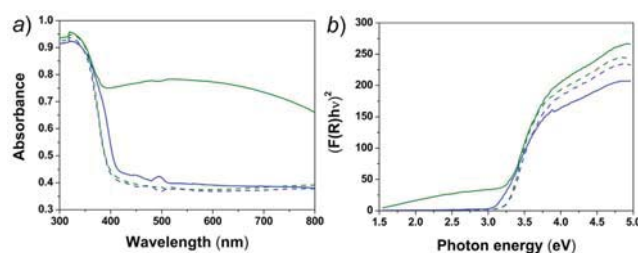
**Figure 7.** *a*) UV/VIS spectra and *b*) plots of (F(R)hν)^2 *vs.* photon energy of PS@TiO$_2$-1 (solid) and PS@TiO$_2$-2 (dashed) after calcination at 500 °C (green) and 700 °C (blue).

Table 3. Band gap energies of PS@TiO$_2$-1 and PS@TiO$_2$-2 after calcination at 500 and 700 °C
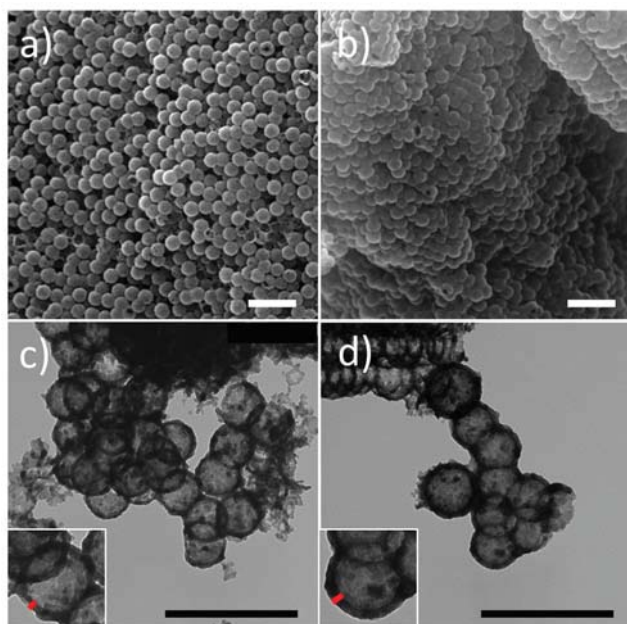
	Temperature of calcination	E_{GAP} [eV]
PS@TiO$_2$-1	500 °C	3.17
	700 °C	3.14
PS@TiO$_2$-2	500 °C	3.26
	700 °C	3.27

The efficiency of the PS dissolution in chloroform was evaluated by increasing the wall thickness of TiO$_2$ (PS@TiO$_2$-2thick). For that, the quantity of PS introduced during the synthesis of PS@TiO$_2$ was divided by a factor 2 (250 mg).

The PS@TiO$_2$-2 and PS@TiO$_2$-2thick particles after dissolution of PS and calcination at 500 °C for 2 h were homogeneous in size and the capsules were undamaged (*Fig. 8a* and *b*). The TEM pictures showed clearly the void inside of the capsules, proving removal pathway's efficiency. The zooms in *Fig. 8c* and *d* show clearly that the wall thickness is increased by increasing the Ti precursor: PS ratio during the synthesis (the red bar represents the thickness of the
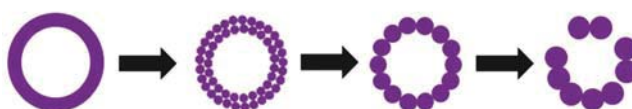
Scheme 2. Proposed process of TiO$_2$ NC crystallization by increasing the calcination temperature.

Figure 9. *a*) Photocatalytic degradation of MB and *b*) *pseudo*-first order kinetics model over PS@TiO$_2$-1 (black square), PS@TiO$_2$-2 (violet triangle) and PS@TiO$_2$-2thick (cyan pentagon) after thermal treatment at 500 °C for 2 h.

Figure 8. SEM and TEM pictures of (*a*, *c*) PS@TiO$_2$-2 and (*b*, *d*) PS@TiO$_2$-2thick after dissolution of PS and calcination at 500 °C for 2 h, scale bar represents 500 nm.
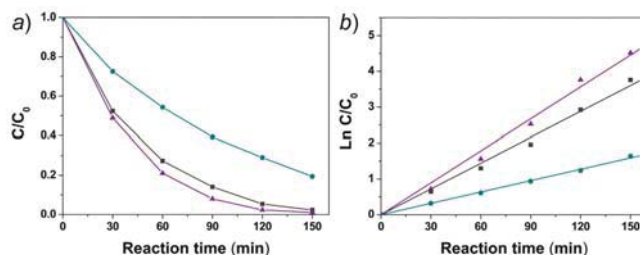
walls of around 20 nm and 30 nm for PS@TiO$_2$-2 and PS@TiO$_2$-2thick, respectively).

Photodegradation of Methylene Blue (MB)

TiO$_2$ has proven to be very effective in the photodegradation of recalcitrant dyes contained in wastewater such as heteropolyaromatic (methylene blue (MB)) or azoic (methyl red, congo red) compounds with a complete mineralization.[30]

The photocatalytic properties of our three different samples PS@TiO$_2$-1, PS@TiO$_2$-2 and PS@TiO$_2$-2thick were evaluated by studying the photodegradation of methylene blue (MB) after thermal treatment of the catalysts at 500 °C for 2 h.

The photocatalytic degradation of MB was followed by UV-visible spectroscopy (*Figs. S3 – S5*) and their profiles are represented in *Fig. 9a*. The use of PS@TiO$_2$-1 obtained from thermal decomposition of PS, which damaged and drilled the TiO$_2$ shell, leads to lower photoactive degradation of MB compared to PS@TiO$_2$-2. We assume that this difference could be explained by the fact that the void space allows an efficient harvesting of the light and this phenomenon would be less important when the structure is disrupted. On the other hand, a drastic drop was noticed when the thickness of the shell was increased (PS@TiO$_2$-2thick). In considering a pseudo first order kinetic model, the constant rate k was evaluated from

the slope of the linear graph shown in *Fig. 9b*. The k rate was respectively 24.0×10^{-3}, 29.7×10^{-3}, and 10.6×10^{-3} min^{-1} for PS@TiO$_2$-1, PS@TiO$_2$-2, and PS@TiO$_2$-2thick, respectively. According to these data, the PS@TiO$_2$-2 was the most active catalyst being three times more photoactive than PS@TiO$_2$-2thick.

Conclusions

This study showed the impact of the polystyrene removal pathway on the structure of titanium oxide nanocapsules from PS@TiO$_2$ core-shell particles. Indeed, the thermal decomposition of polystyrene simultaneously with the titanium dioxide crystallization implied the destruction of the capsules as starting from 300 °C while the dissolution of the polystyrene followed by the thermal crystallization of the titanium oxide allowed the preservation of the TiO$_2$ nanocapsule structure until at least 500 °C. In both PS removal pathways, the capsular shape of the TiO$_2$ is lost at 700 °C. At this temperature, the collapse of the TiO$_2$ structure was probably not due to the removal of the polystyrene but rather originated from the crystallization process of the TiO$_2$, where the crystallite size reached the TiO$_2$ nanocapsules wall thickness.

For the photodegradation of MB, the removal pathway of PS influences the photoactivity, but compared to this, the TiO$_2$ wall thickness is a predominant parameter in the photoactivity.

Experimental Section

Polystyrene Synthesis

The anionic polystyrene beads (PS) were synthetized following a microemulsion method from *Kartsonakis et al.*[24]

To avoid the side reaction with oxygen, the formation of PS was carried out under inert atmosphere (N$_2$). In a reflux system, sodium dodecylsulfate (0.09 g, 0.3 mmol) used as surfactant and potassium persulfate

(0.30 g, 1.1 mmol) used as initiator were introduced in water (250 ml) and mixed together during 30 min under inert atmosphere. The styrene (3.70 g, 35.5 mmol) was added and the reaction mixture was kept at 80 °C for 42 h. Then, the mixture was centrifuged to remove the supernatant. The PS was washed three times with water (by washing/centrifuging steps) and was resuspended in a small amount of water for the storage.

PS@TiO₂ Core-Shell Synthesis

The titanium oxide shell formation was inspired from the hydrolysis synthesis of *Imhof*.[10]

Typically, two solutions were prepared separately. In the first one, the polyvinylpyrrolidone (0.672 g) and a solution of NaCl (1.675 ml, 5 mM) were successively introduced in ethanol (73 ml) containing the polystyrene beads (500 mg) under vigorous stirring. In the second one, the titanium isopropoxide (0.756 ml) was mixed in ethanol (10 ml) under vigorous stirring.

Then the second solution was rapidly introduced in the suspension containing PS at 500 rpm. The stirring was kept for 1 min, and the suspension was aged for 14 min more.

Finally, the supernatant was removed and the PS@TiO₂ was washed three times with ethanol by centrifuging and dried at 50 °C overnight.

Removing PS Core Processes

Two pathways were compared to remove the PS core *i*) by thermal decomposition of PS under air and *ii*) by dissolution of PS into chloroform.

Thermal Decomposition of PS Core (PS@TiO₂-1)

The PS@TiO₂ materials were calcined at different temp. to follow the decomposition of PS, obtaining by this way TiO₂ nanocapsule (NC). Several batches were introduced in a cubic furnace and they were progressively removed after reaching the appropriate temp. (300, 400, 500 and 700 °C) using a ramp of 5 °C/min.

Dissolution of PS Core (PS@TiO₂-2)

In *Soxhlet* apparatus, the PS@TiO₂ was placed into the cellulose extraction thimbles and the chloroform was introduced into the flask. The solvent was refluxed for 4 to 5 h to pass through the PS@TiO₂ and dissolve the polystyrene. Then the solid (TiO₂ NC) was rinsed with ethanol and dried at 50 °C overnight.

The same thermal study than the thermal decomposition process was realized after the PS dissolution.

Characterizations

The TGA analysis was performed with *Mettler Toledo TGA/SDTA851e* from 25 to 600 °C using a ramp of 5 °C/min. The infrared spectra were collected with *Frontier* FT-IR spectrometer from *PerkinElmer* in ATR mode. The Powder X-Ray diffractograms were recorded in transmission mode with a *Stoe STADIP* equipped with copper monochromator source and *Mythen* detector. The samples were introduced into a 0.5 mm diameter capillary. For the Scanning Electron Microscopy, the samples were deposited onto a carbon tape and sputtered with 4 nm thickness gold. The analysis was performed with a *TESCAN Mira 3 LM* field emission. The TEM picture was recorded with a *Philips CM100 Biotwin*. The solid-state measurement of UV-visible spectra was recorded in *PerkinElmer 900 UV/VIS* Spectrometer equipped with integrating sphere.

Photodegradation of Methylene Blue (MB)

In a 2 cm quartz cuvette filled with 5 ml of MB (84.2 µmol/l in water), 2.5 mg of the catalyst was added and resuspended using an ultrasonic bath.

The cuvette was covered in dark for 30 min to reach the MB adsorption/desorption equilibrium on the surface of the catalyst. The suspension was then exposed to a mercury lamp with 335 nm cut off filter for 150 min. Every 30 min, a 0.6 ml aliquot was taken off and put into the centrifuge to settle down the particles; then 0.5 ml of the supernatant was introduced in a 1 cm quartz cuvette and filled with 1.5 ml of deionized water. The solution was analyzed by UV-vis spectroscopy in a *PerkinElmer Lambda 2S* UV/VIS Spectrometer. During the whole photocatalytic reaction, the temp. of the suspension was maintained at around 15 °C with a recirculating cooler.

Supplementary Material

Supporting information for this article is available on the WWW under https://doi.org/10.1002/hlca.201700014.

Acknowledgements

Author Contribution Statement

Dr. *Nelly Hérault* performed the synthesis and analysis on all samples, interpreted the data, and wrote manuscript. Prof. *K. M. Fromm* supervised the development of work, helped in data interpretation, manuscript evaluation, and corrections.

References

[1] J. Hu, M. Chen, X. Fang, L. Wu, 'Fabrication and application of inorganic hollow spheres', *Chem. Soc. Rev.* **2011**, *40*, 5472 − 5491.

[2] J. Cai, Z. Wang, K. Lv, Y. Zheng, J. Yu, M. Li, 'Rapid synthesis of a TiO_2 hollow microsphere assembly from hollow nanoparticles with enhanced photocatalytic activity', *RSC Adv.* **2013**, *3*, 15273 − 15281.

[3] Z. Zhong, Y. Yin, B. Gates, Y. Xia, 'Preparation of Mesoscale Hollow Spheres of TiO_2 and SnO_2 by Templating Against Crystalline Arrays of Polystyrene Beads', *Adv. Mater.* **2000**, *12*, 206 − 209.

[4] I. Tissot, J. P. Reymond, F. Lefebvre, E. Bourgeat-Lami, 'SiOH-Functionalized Polystyrene Latexes. A Step toward the Synthesis of Hollow Silica Nanoparticles', *Chem. Mater.* **2002**, *14*, 1325 − 1331.

[5] S. M. Mousavi, A. R. Mahjoub, R. Abazari, 'Green synthesis of ZnO hollow sphere nanostructures by a facile route at room temperature with efficient photocatalytic dye degradation properties', *RSC Adv.* **2015**, *5*, 107378 − 107388.

[6] S. Peng, S. Sun, 'Synthesis and Characterization of Monodisperse Hollow Fe_3O_4 Nanoparticles', *Angew. Chem., Int. Ed.* **2007**, *46*, 4155 − 4158.

[7] J. Gagnon, M. J. D. Clift, D. Vanhecke, D. A. Kuhn, P. Weber, A. Petri-Fink, B. Rothen-Rutishauser, K. M. Fromm, 'Integrating silver compounds and nanoparticles into ceria nanocontainers for antimicrobial applications', *J. Mater. Chem. B* **2015**, *3*, 1760 − 1768.

[8] A.-H. Pei, Z.-W. Shen, G.-S. Yang, 'Preparation of TiO_2 nanocapsules for loading and release of antimicrobial triclosan molecules', *Mater. Lett.* **2007**, *61*, 2757 − 2760.

[9] R. Yang, H. Li, X. Qiu, L. Chen, 'A Spontaneous Combustion Reaction for Synthesizing Pt Hollow Capsules Using Colloidal Carbon Spheres as Templates', *Chem. Eur. J.* **2006**, *12*, 4083 − 4090.

[10] A. Imhof, 'Preparation and Characterization of Titania-Coated Polystyrene Spheres and Hollow Titania Shells', *Langmuir* **2001**, *17*, 3579 − 3585.

[11] T. Leshuk, S. Linley, G. Baxter, F. Gu, 'Mesoporous Hollow Sphere Titanium Dioxide Photocatalysts through Hydrothermal Silica Etching', *ACS Appl. Mater. Interfaces.* **2012**, *4*, 6062 − 6070.

[12] T. Yang, J. Liu, R. Zhou, Z. Chen, H. Xu, S. Z. Qiao, M. J. Monteiro, 'N-doped mesoporous carbon spheres as the oxygen reduction reaction catalysts', *J. Mater. Chem. A* **2014**, *2*, 18139 − 18146.

[13] A. W. Tan, B. Pingguan-Murphy, R. Ahmad, S. A. Akbar, 'Review of titania nanotubes: Fabrication and cellular response', *Ceram. Int.* **2012**, *38*, 4421 − 4435.

[14] S.-Y. Lee, S.-J. Park, 'TiO_2 photocatalyst for water treatment applications', *J. Ind. Eng. Chem.* **2013**, *19*, 1761 − 1769.

[15] K. Nakata, A. Fujishima, 'TiO_2 photocatalysis: Design and applications', *J. Photochem. Photobiol. C* **2012**, *13*, 169 − 189.

[16] D. Chen, F. Huang, Y.-B. Cheng, R. A. Caruso, 'Mesoporous Anatase TiO_2 Beads with High Surface Areas and Controllable Pore Sizes: A Superior Candidate for High-Performance Dye-Sensitized Solar Cells', *Adv. Mater.* **2009**, *21*, 2206 − 2210.

[17] T.-H. Zhang, L.-Y. Piao, S.-L. Zhao, Z. Xu, Q. Wu, C. Kong, 'Application of TiO_2 with different structures in solar cells', *Chin. Phys. B* **2012**, *21*, 118401.

[18] G. Siddiqi, V. Mougel, C. Copéret, 'Highly Active Subnanometer Au Particles Supported on TiO_2 for Photocatalytic Hydrogen Evolution from a Well-Defined Organogold Precursor, $[Au_5(mesityl)_5]$', *Inorg. Chem.* **2016**, *55*, 4026 − 4033.

[19] M. Ni, M. K. H. Leung, D. Y. C. Leung, K. Sumathy, 'A review and recent developments in photocatalytic water-splitting using TiO_2 for hydrogen production', *Renew. Sust. Energ. Rev.* **2007**, *11*, 401 − 425.

[20] Y. Ma, X. Wang, Y. Jia, X. Chen, H. Han, C. Li, 'Titanium Dioxide-Based Nanomaterials for Photocatalytic Fuel Generations', *Chem. Rev.* **2014**, *114*, 9987 − 10043.

[21] M. N. Chong, B. Jin, C. W. K. Chow, C. Saint, 'Recent developments in photocatalytic water treatment technology: A review', *Water Res.* **2010**, *44*, 2997 − 3027.

[22] W. J. Tseng, P.-S. Chao, 'Synthesis and photocatalysis of TiO_2 hollow spheres by a facile template-implantation route', *Ceram. Int.* **2013**, *39*, 3779 − 3787.

[23] A. F. Demirörs, van Blaaderen A., A. Imhof, 'A General Method to Coat Colloidal Particles with Titania', *Langmuir* **2010**, *26*, 9297 − 9303.

[24] I. A. Kartsonakis, P. Liatsi, I. Daniilidis, G. Kordas, 'Synthesis, Characterization, and Antibacterial Action of Hollow Ceria Nanospheres with/without a Conductive Polymer Coating', *J. Am. Ceram. Soc.* **2008**, *91*, 372 − 378.

[25] A.-Y. León-Bermúdez, R. Salazar, 'Synthesis and characterization of the polystyrene-asphaltene graft copolymer by FT-IR spectroscopy', *Ciencia, Tecnología y Futuro* **2008**, *3*, 157 − 167.

[26] N. Sharotri, D. Sud, 'Ultrasound-assisted synthesis and characterization of visible light responsive nitrogen-doped TiO_2 nanomaterials for removal of 2-Chlorophenol', *Desalin. Water Treat.* **2016**, *57*, 8776 − 8788.

[27] D. A. H. Hanaor, C. C. Sorrell, 'Review of the anatase to rutile phase transformation', *J. Mater. Sci.* **2011**, *46*, 855 − 874.

[28] P. Kubelka, F. Munk, 'Ein Beitrag zur Optik der Farbanstriche', *Z. techn. Phys.* **1931**, *12*, 593 − 601.

[29] M. L. Myrick, M. N. Simcock, M. Baranowski, H. Brooke, S. L. Morgan, J. N. McCutcheon, 'The Kubelka-Munk Diffuse Reflectance Formula Revisited', *Appl. Spectrosc. Rev.* **2011**, *46*, 140 − 165.

[30] H. Lachheb, E. Puzenat, A. Houas, M. Ksibi, E. Elaloui, C. Guillard, J.-M. Herrmann, 'Photocatalytic degradation of various types of dyes (Alizarin S, Crocein Orange G, Methyl Red, Congo Red, Methylene Blue) in water by UV-irradiated titania', *Appl. Catal. B* **2002**, *39*, 75 − 90.

[31] M. T. García, I. Gracia, G. Duque, A. Lucas, J. F. Rodríguez, 'Study of the solubility and stability of polystyrene wastes in a dissolution recycling process', *Waste Manage.* **2009**, *29*, 1814 − 1818.